THE JOURNAL OF PHYSICAL CHEMISTRY C

Article

pubs.acs.org/JPCC

A Surface Hopping View of Electrochemistry: Non-Equilibrium Electronic Transport through an Ionic Solution with a Classical Master Equation

Wenjun Ouyang, Jeffery G. Saven, and Joseph E. Subotnik*

Department of Chemistry, University of Pennsylvania, 231 South 34 Street, Philadelphia, Pennsylvania 19104-6323, United States

Supporting Information

ABSTRACT: We use a recent flavor of surface hopping dynamics to investigate the non-equilibrium transport of electrons as carried by a few ions through a solution of Lennard-Jones spheres across a finite voltage. We analyze our nonequilibrium results through a combination of equilibrium simulations and steady state rate equations. While the non-equilibrium dynamics approach in this paper is computationally demanding and likely limited to reasonably small simulation sizes (or short time scales), the present study does provide a simple means for us to understand the interplay between nuclear motion near a metal surface and charge injection into/from the metal surface. This interplay is especially interesting when the system of interest is far from the linear response regime (which might well be very common in electrochemistry).

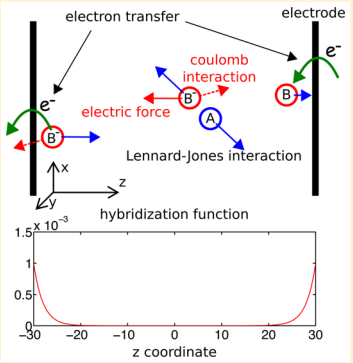

1. INTRODUCTION

The field of electrochemistry is an area of physical chemistry where the theoretical tools are unfortunately limited. By its very nature, electrochemistry is difficult to model atomistically: one must treat the nuclear motion of solute and solvent molecules (including mass transport over long distances), the electronic and nuclear dynamics of the metal electrode, and electron transfer at the electrode interface. As such, simulating electrochemistry is difficult.[1] That being said, the field of electrochemistry touches upon so many interesting phenomena—corrosion, battery lifetimes, aluminum production, biosensors, fuel cells, etc.—that it is worthwhile developing new and approximate theoretical tools.

In practice, for our purposes, it is convenient to consider electrochemistry as the combination of two different phenomena. First, in many electrochemistry experiments, chemical reactions occur at a metal electrode; some covalent bonds are broken, some are created. Second, at an electrochemical interface, there will be electron transfer between a metal electrode and a molecular species in solution. And this electron transfer can come in different flavors: either outer sphere electron transfer (where metal-molecule coupling is weak) or inner sphere electron transfer (where metal−molecule coupling is strong). Below, we will focus mostly on outer sphere electron transfer; we will only briefly discuss the role of breaking/making bonds in section 5.2.

Our goal in the present paper is to model the solution-phase flow of electrons through a simple electrochemical setup. See Figure 1. In particular, we want to model the following three steps: (*i*) electrons hop from one metal electrode surface (cathode on the right) onto solute charge carriers in solution, (*ii*) charged ions drift through an ambient liquid, (*iii*) electrons leave the solute charge carriers and hop onto a metal electrode surface (anode on the left), thus completing a cycle of reduction and oxidation of the charge carrier. From the point of view of physical chemistry, most research in electrochemistry has traditionally focused on the statistical mechanics of the ions near the electrode interface (screening, e.g.[2]) rather than dynamics. In this paper, our main focus is on treating the quantum processes in steps *i* and *iii*.

To achieve this goal of explicitly addressing charge injection, we will run dynamics on a fluctuating stochastic potential. Consider a molecule that can be either charged or uncharged near a wide-band metal.[3] Without loss of generality, we assume the charge-carrier molecule starts off neutral (at time 0) and we run classical dynamics for the neutral molecule for some period of initialization time. Thereafter, we allow stochastic changes in the charge state of the molecule, which will in turn change the molecule's local environment and vibrational frequencies. The details of when we change charge states are described below (and in ref 4).

From the perspective of chemistry, the stochastic algorithm just described can be considered a member of the surface hopping family, in the same spirit as the original Tully algorithm.[5] However, whereas the original Tully algorithm was applied to systems with only a few electronic states, the present algorithm concerns surface hopping with a continuum of electronic states.

Received: July 10, 2015
Revised: August 12, 2015

DOI: 10.1021/acs.jpcc.5b06655
J. Phys. Chem. C XXXX, XXX, XXX−XXX

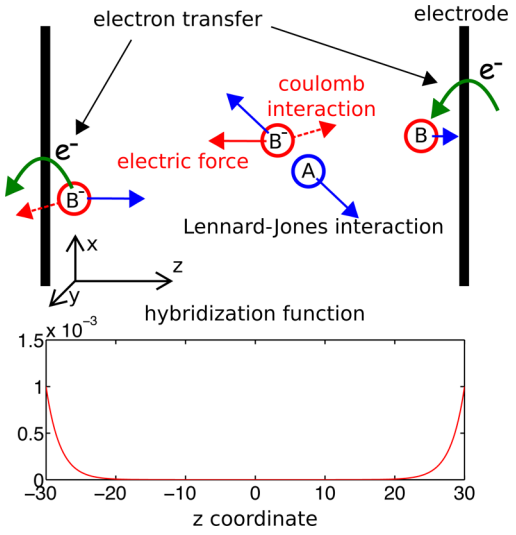

Figure 1. (Top) Schematic picture of our system. The blue open circles labeled "A" denote solvent atoms and the red open circles labeled "B" or "B^-" denotes solute atoms. Solute atoms can be neutral ("B") or charged ("B^-"). The Lennard-Jones interaction is shown with blue arrows, the electric force due to the electric field is represented by a red arrow, and the long-range Coulomb interactions between charged B^- atoms is shown with dashed red arrows. The direction of electron transfer is illustrated with a curved green arrow. (Bottom) Electronic hybridization function as a function of z (which is also known as the electronic broadening, $\Gamma(z)/h$; see eq 11).

As such, there are key distinctions between the two surface hopping algorithms.

- Tully's surface hopping algorithm (e.g., for two states) propagates classical nuclei along adiabatic surfaces while keeping track of the electronic coherences with an auxiliary set of amplitudes. Electronic hops are accompanied by momentum adjustments to maintain energy conservation, and for accuracy, electronic decoherence must be included on top of the Tully scheme.[6−25]
- The present algorithm for many states propagates nuclei along diabatic potential energy surfaces corresponding to different charge states of the molecule and does not propagate any electronic coherence at all (because we assume the wide band limit for the metal surface). According to the present algorithm, individual trajectories do not maintain energy conservation and there are no momentum adjustments.

Nevertheless, despite these differences, both the Tully and the present approach follow the same rules roughly: classical nuclear motion along static (not mean-field) potential energy surfaces with hops between surfaces to account for nonadiabatic relaxation. Furthermore, both approaches recover detailed balance, either approximately (in the case of the Tully algorithm[26,27]) or exactly (in the case of the present algorithm). In practice, the need to go beyond Tully's original algorithm is dictated only by computational cost: running Tully dynamics over a continuum of adiabatic electronic states would be astronomically expensive (though approximations can be made[28−30]). This statement about computational cost would be true for most other quantum or mixed quantum-classical methods[31−42] if they treat the electronic bath explicitly. In short, the present many-body version of surface hopping was designed to treat an open quantum system with minimal cost.

Now, from the perspective of molecular conduction, the many-body surface hopping algorithm just described can be (and was) derived[43] in a straightforward fashion by (*i*) assuming the metal-molecule coupling is small (in the spirit of outer-sphere electrochemistry) which leads to a master equation, and (*ii*) assuming the temperature is large enough that all nuclear motion can be considered classical. Thus, our surface hopping algorithm can be considered a "classical master equation", which guarantees that the method evolves to recover the correct equilibrium distribution. Naturally, this approach should be valid in the limit of outer sphere electrochemistry, i.e. electron transfer between a metal surface and molecules that are close by, but not covalently attached.[4] Given the interdisciplinary nature of electrochemistry, it is perhaps not surprising that simple techniques in one area of physics (molecular conduction through molecules) will be useful in a very different area of chemistry (solution-phase charge carrier transport). After all, there is a long history of nonequilibrium chemical dynamics in statistical physics.[44,45]

Interestingly, recently Voth and co-workers[46,47] performed related nonequilibrium simulations to capture the flow of ions through a solution of electrolytes across a voltage. The algorithm in the present paper can effectively be considered an atomistic version of the Voth coarse-grained scheme in refs 46 and 47, which evaluates hopping probabilities with an averaged Marcus rate and does not allow back transfer. The method proposed herein explicitly allows back electron transfer and uses an atomistic electron transfer rate while assuming no averaging of the transfer rate. While Voth et al. treat the problem of the image charge properly, in the present paper, we treat the effect of the image charge only heuristically—just enough to ensure that we extract the proper physics.

Finally, our aim is to study ionic conduction. Our plan of attack is as follows. We consider a liquid made up of solvent and redox-active solute atoms. We will simulate the ionic current through the liquid using both fully nonequilibrium molecular dynamics and a combination of equilibrium dynamics with chemical kinetics. We will investigate how and when the latter matches the former. Our paper is organized as follows. Section 2 defines our model Hamiltonian, outlines the details of our nonequilibrium algorithm, and reviews the working equations for estimating current with linear response. Section 3 provides all the necessary atomistic details about our simulation. Section 4 analyzes our simulation results and makes a comparison between nonequilibrium and equilibrium dynamics. Section 5 separates mass transport versus electron transfer contributions to the final current. Section 6 concludes the paper.

2. THEORY

For the notation we let q be the charge of an ion and e be the charge of an electron, so that q/e is dimensionless.

2.1. The Model Hamiltonian. Our model system is a slab system consisting of two parallel plane electrodes separated in the z direction. Periodic boundary conditions are applied in the x and y directions (not z). We consider two classes of atoms: solvent atoms ("A") and charge carrier solute atoms ("B"). The total Hamiltonian of the system is the following:

$$H(\mathbf{r}^{(A)}, \mathbf{r}^{(B)}, \mathbf{v}^{(A)}, \mathbf{v}^{(B)}, q^{(B)}) \equiv E_k + U_{AA} + U_{AB} + U_{BB} + U_{electrode} + U_{field} + U_{atomic} \quad (1)$$

DOI: 10.1021/acs.jpcc.5b06655
J. Phys. Chem. C XXXX, XXX, XXX−XXX

where E_k is the total kinetic energy, $\mathbf{r}$ and $\mathbf{v}$ are the sets of 3D coordinates and velocities of a particular atom type, and q is the charge on B atoms. A schematic figure of the system is shown in Figure 1, where we also indicate the pairwise interactions and the hybridization function for electron transfer.

2.1.1. A–A and A–B Interactions. Since the A atoms are neutral, the A–A and A–B interactions are chosen to be simple Lennard-Jones interactions whether B is neutral or charged:

$$U_{AA} = \sum_{i<j} 4\varepsilon_{AA}\left[\left(\frac{\sigma_{AA}}{|\mathbf{r}_i^{(A)} - \mathbf{r}_j^{(A)}|}\right)^{12} - \left(\frac{\sigma_{AA}}{|\mathbf{r}_i^{(A)} - \mathbf{r}_j^{(A)}|}\right)^{6}\right] \quad (2)$$

$$U_{AB} = \sum_{i<j} 4\varepsilon_{AB}\left[\left(\frac{\sigma_{AB}}{|\mathbf{r}_i^{(A)} - \mathbf{r}_j^{(B)}|}\right)^{12} - \left(\frac{\sigma_{AB}}{|\mathbf{r}_i^{(A)} - \mathbf{r}_j^{(B)}|}\right)^{6}\right] \quad (3)$$

where $\mathbf{r}_i^{(A)}$ and $\mathbf{r}_j^{(B)}$ are the coordinates of A and B atoms labeled i and j. The sum in each case is restricted to A–A and A–B pairs. For simplicity in this study, we assume that A and B are identical with respect to these interactions: $\varepsilon_{AA} = \varepsilon_{AB} = \varepsilon$ and $\sigma_{AA} = \sigma_{AB} = \sigma$. For simplicity of notation, we define the pair potential U_{LJ}:

$$U_{LJ}(r) = 4\varepsilon\left[\left(\frac{\sigma}{r}\right)^{12} - \left(\frac{\sigma}{r}\right)^{6}\right] \quad (4)$$

Here ε and σ are the Lennard-Jones constants.

2.1.2. B–B Interaction. A solute (B) atom can be charged or neutral. Let q_i and q_j be the charges on two atoms. The B–B interaction is defined as a Lennard-Jones interaction plus a Coulomb interaction.

$$U_{BB} = \sum_{i<j} U_{BB}(\mathbf{r}_i^{(B)}, \mathbf{r}_j^{(B)}) \quad (5)$$

$$U_{BB}(\mathbf{r}_i^{(B)}, \mathbf{r}_j^{(B)}) \equiv U_{LJ}(|\mathbf{r}_i^{(B)} - \mathbf{r}_j^{(B)}|) + \frac{q_i q_j}{4\pi\epsilon|\mathbf{r}_i^{(B)} - \mathbf{r}_j^{(B)}|} \quad (6)$$

Here ϵ is the permittivity. Note that if one or both of the solute atoms is neutral, $U_{BB} = U_{LJ}$.

2.1.3. Electrode–A and Electrode–B Interactions. We represent each electrode as a simple planar surface with respect to its interactions with the atoms in the liquid. The interaction between electrodes and an A atom or a B atom is a Lennard-Jones interaction defined above in eq 4. If $z^{(L)}$ is the z-coordinate for the left electrode, $U_{electrode}^{(LA)}(\mathbf{r}^{(A)}) \equiv U_{LJ}(|z^{(A)} - z^{(L)}|)$. All other atom–electrode potentials are defined analogously.

2.1.4. Interaction with External Electric Field. The relationship between the voltage (V) and the electrochemical potential (μ) of the left (L) and right (R) electrodes is defined as

$$V_L \equiv \frac{\mu_L}{e}, \quad V_R \equiv \frac{\mu_R}{e}, \quad V \equiv V_L - V_R \quad (7)$$

where e is the electron charge (negative). The external electric field can be calculated from the voltage between the two electrodes:

$$\mathcal{E} \equiv \frac{V}{L_z} = \frac{V_L - V_R}{L_z} = \frac{\mu_L - \mu_R}{eL_z} \quad (8)$$

where L_z is the distance between the two electrodes. When the voltages V_L and V_R at the two electrodes are different—or equivalently the electrochemical potentials for electrons μ_L and μ_R differ—the applied electric field will interact with charged B^- atoms. The potential energy due to the electric field is

$$U_{field} = \sum_i U_{field}(z_i^{(B)}) \equiv \sum_i \left(\mu_L + \frac{\mu_R - \mu_L}{L_z}(z_i^{(B)} - z^{(L)})\right)\frac{q_i}{e} \quad (9)$$

2.1.5. Electron Affinity. The electron affinity energy is included in the term U_{atomic} in eq 1. Note that we do not include ionization energy in eq 1 because we do not have a positive charge carrier in our system for simplicity. In the future, it will be interesting to have two types of charge carriers, negative and positive.

2.2. Boundary Conditions and Electron transfer. Let us now discuss the boundary conditions at the electrode, where B atoms can accept charge from the metal and B^- can donate a charge to the metal. Our approach will be based on the classical master equation and surface hopping dynamics presented in refs 4 and 43. The model is very simple: if the i^{th} solute atom (B_i) accepts an electron (making B_i^-), then the charge q_i changes from 0 to e in eq 6 and eq 9 and the system evolves accordingly. Vice versa, if the ith solute atom (B_i^-) donates an electron (making B_i), then the charge q_i changes from e to 0.

The probability for a neutral solute atom (B) to accept an electron from the left metal is

$$\zeta_{accept}(\Delta z_L, \Delta H) = \mathrm{d}t\,\frac{\Gamma(\Delta z_L)}{\hbar}\frac{1}{1 + \exp(\beta(\Delta H - \mu_L q/e))} \quad (10)$$

where dt is the time span in which electron transfer is considered, Δz_L is the absolute distance between the atom and the left electrode, $\beta = 1/(k_b T)$. For the electron transfer probability for the right electrode, one substitutes R for L. $\Gamma(z)$ is the position dependent hybridization function defined as

$$\Gamma(z) = \Gamma_0 \exp(-z/\lambda) \quad (11)$$

The parameter Γ_0 denotes the strength of coupling when the solute sits at the metal surface, and λ is the decay parameter for the coupling in space (also known as β^{-1} for electron transfer in molecules[3]). ΔH is the change in energy (see eq 1) after the charge is accepted, to which we add the effect of a new image charge:

$$\Delta H = H(\mathbf{r}, \mathbf{v}, q_1, q_2, \cdots, q_i = e, \cdots, q_{N_B}) - H(\mathbf{r}, \mathbf{v}, q_1, q_2, \cdots, q_i = 0, \cdots, q_{N_B}) + \Delta U_{image} \quad (12)$$

ΔU_{image} must be included in eq 12 because image charges in the metal will adjust very quickly to the appearance of a B^- atom, and the effect of such an image charge need not be small if a B^- atom is close to an electrode. In truth, an optimal algorithm should actually evaluate all image charges (corresponding to all charged B^- atoms) at every time step as part of the Hamiltonian eq 1—not just when a B atom approaches a surface and accepts a charge. Calculating the locations and fields of all image charges (on both conducting electrodes) is possible[48] and has been achieved by Voth et al.[46] For now, though, and for the sake of simplicity, we presume that image charge effects will be significant only near the electrode surface and we include such effects only through eq 12.[49] Thus, for example, when B accepts a charge from the left electrode, to first order, we assume

$$\Delta U_{image} = \mu_L \frac{-q}{e} \quad (13)$$

DOI: 10.1021/acs.jpcc.5b06655
J. Phys. Chem. C XXXX, XXX, XXX–XXX

To complete the story, the probability for a charge B^- to donate an electron to the left electrode is completely analogous to eq 10

$$\zeta_{donate}(\Delta z_L, \Delta H) = \mathrm{d}t\,\frac{\Gamma(\Delta z_L)}{\hbar}\left(1 - \frac{1}{1+\exp(\beta(\Delta H - \mu_L q/e))}\right) = \mathrm{d}t\,\frac{\Gamma(\Delta z_L)}{\hbar}\frac{1}{1+\exp(\beta(\mu_L q/e - \Delta H))} \tag{14}$$

and similarly for the right electrode.

Finally, we make one comment on periodicity in the x and y directions. In principle, we should use fully two-dimensional periodic boundary conditions in the x, y directions to eliminate spurious wall effects where there is no electrode. That being said, in practice, simulating 2D periodic boundary conditions for long-range Coulombic interactions (that cannot be truncated) in a charged box is tedious; Ewald summation in two dimensions with a charged unit cell is possible but not trivial.[50−53] Thus, for this paper, we will take a short-cut and calculate the direct Coulomb interaction only between a given atom and the closest periodic image of another atom (the minimum image convention[54]); this prescription should be accurate enough with only a few charged particles present simultaneously in the system.

2.3. Algorithm. A step-by-step outline of our simulation algorithm is as follows:

1 Initialize the model system.
   a Initialize for each atom its position ($\mathbf{r}_i$), velocity ($\mathbf{v}_i$), charge (q_i), atomic mass (m_i) and Lennard-Jones constants (σ and ε).
   b Fix the value of the electrochemical potentials μ_L and μ_R.
2 Propagate each atom and a Nosé thermostat[55] using the velocity Verlet algorithm.[56] The forces are obtained by calculating the negative gradient of the total Hamiltonian in eq 1:

$$F(\mathbf{r}) = -\nabla_{\mathbf{r}} H \tag{15}$$

3 Evaluate the probability for electron transfer between the electrodes and a charge carrier. Loop over all charge carriers (i.e., B atoms):
   a Calculate ΔH with eq 12.
   b If B is charged, use eq 14 to calculate the probability $\zeta^{(L)}_{donate}$ for charge donation ($B^- \rightarrow B$) to the left electrode (and the analogous probability for the right electrode $\zeta^{(R)}_{donate}$). Generate a random number g sampled from [0,1]. If $g < \zeta^{(L)}_{donate}$, B^- donates the electron to the left electrode. Otherwise if $g < \zeta^{(L)}_{donate} + \zeta^{(R)}_{donate}$, B^- donates the electron to the right electrode. Go to step 3d.
   c If B is neutral, use eq 10 to calculate the probability $\zeta^{(L)}_{accept}$ for charge acceptance ($B \rightarrow B^-$) from the left electrode (and the analogous probability for the right electrode ζ^{R}_{accept}). Generate a random number g sampled from [0,1]. If $g < \zeta^{(L)}_{accept}$, B accepts the electron from the left electrode. Otherwise if $g < \zeta^{(L)}_{accept} + \zeta^{(R)}_{accept}$, B accepts the electron from the right electrode. Go to step 3d.
   d If an electron transfer event occurs, update the charges as used in eq 1 and eq 15.
4 Continue to step 2.

2.4. Linear Response Theory. With equal electrochemical potentials on both left and right electrodes (i.e., no voltage, $V = 0$), the methodology just described is essentially a sampling of the grand canonical ensemble for charge carrier species B and B^-.[57] The only nuance here is that, in the course of a Monte Carlo simulation, we add/subtract charges according to a position dependent criteria based on $\Gamma(z)$—whereas the insertion rate is usually treated as a constant.[57] That being said, many interesting phenomena appear when we have different electrochemical potentials on two electrodes (e.g., a current).

Within the context of equilibrium statistical mechanics, linear response theory (and specifically the Green−Kubo relation) is a powerful tool for estimating the conductivity of the system. According to linear response, if we denote the perturbation to the equilibrium system as $H_1 = \mathcal{E}qz$, then to first order of βH_1, the response of the system is proportional to the time integral of the velocity autocorrelation function as calculated from an equilibrium simulation. The mobility u is then calculated to be[3]

$$u = \beta\int_0^\infty \mathrm{d}t\,\left\langle v_z(0)v_z(t)\right\rangle = \frac{\beta}{3}\int_0^\infty \mathrm{d}t\left\langle \mathbf{v}(0)\cdot\mathbf{v}(t)\right\rangle \tag{16}$$

More generally, if we define the current density $\mathbf{J}$

$$\mathbf{J}(\mathbf{r}, t) = \frac{q\sum_j \mathbf{v}_j(t)\delta(\mathbf{r}-\mathbf{r}_j)}{V} \tag{17}$$

where V is the volume of the system, eq 16 becomes the Green−Kubo expression for conductivity:

$$\sigma_c = \frac{\beta}{3}\int \mathrm{d}\mathbf{r}\int_0^\infty \mathrm{d}t\,\langle \mathbf{J}(0,0)\cdot\mathbf{J}(\mathbf{r},t)\rangle \tag{18}$$

In practice, below we would like to compare (i) the current as calculated with our nonequilibrium surface hopping approach versus (ii) the current as calculated with linear response. To make this comparison, we have calculated and integrated the velocity-velocity correlation function in eq 16.[58]

With this in mind, the conductance ($G = I/V$, the inverse of resistance) is calculated as follows. First, we calculate the conductivity:

$$\langle J_z\rangle = \sigma_c\mathcal{E}_z = \rho_q e\langle v_z\rangle = \rho_q e^2 u\mathcal{E}_z \tag{19}$$

$$\Rightarrow \sigma_c = \rho_q u e^2 \tag{20}$$

where ρ_q is the density of B^- atoms, $\mathcal{E}_z = \mathcal{E}$ is the electric field, and u is the mobility defined in eq 16. Second, the conductance of our system is

$$G = \sigma_c\frac{S_{xy}}{L_z} = \rho_q u e^2\frac{S_{xy}}{L_z} = ue^2\frac{N_q}{\mathcal{V}}\frac{S_{xy}}{L_z} \tag{21}$$

where S_{xy} is the cross-sectional area in xy plane of our system. Here $\rho_q \equiv N_q/\mathcal{V}$. N_q is the total number of B^- atoms in the system and $\mathcal{V}$ is the effective volume of the system ($\mathcal{V} < V$):

$$\mathcal{V} = S_{xy}L_z^{(eff)} \tag{22}$$

$L_z^{(eff)}$ is the system's effective length in the z-direction. Because of the repulsion between atoms and electrodes at short distances (according to a Lennard-Jones potential), we should expect $L_z^{(eff)} < L_z$, where L_z is the total distance between two electrodes. In practice, $L_z^{(eff)}$ is calculated by measuring the

DOI: 10.1021/acs.jpcc.5b06655
J. Phys. Chem. C XXXX, XXX, XXX−XXX

distance between the two peaks closest to the left and right electrodes in Figure 5a.

In the end, eq 21 leads to

$$G = \frac{ue^2 N_q}{L_z L_z^{(eff)}}, \quad I = GV \tag{23}$$

eq 23 will be used below to estimate the current of our system according to linear response theory.

3. ATOMISTIC DETAILS

For our simulation cell, the two electrodes extend along the *xy* plane between $z = \pm 30$ Å, and the cell length is 20 Å in both the *x* and *y* directions. Between the electrodes, there are 490 "argon" (A) atoms and the charge carriers are modeled by 14 "fluorine" (B) atoms. For the sake of simplicity, all atoms share the same Lennard-Jones constants as those of argon atom: $\sigma = 3.405$ Å and $\varepsilon = 0.2379$ kcal/mol (see eq 4). The mass of the A atoms is 39.948 amu and the mass of the B atoms is 18.998 amu. For computational convenience, we use the minimum image convention[54] for both Coulomb and Leonard Jones interactions, whereby each atom interacts with only one (i.e., the closest) of the periodic images of another atom. For simplicity, we truncate all Lennard-Jones interactions at 8.5 Å in eq 1. For the Coulomb interaction between B^- atoms, the permittivity is set as $\epsilon = 80\epsilon_0$, i.e., water. Our system is thermostated[55] at 300 K. For the electron transfer, the strength of electronic coupling is chosen such that the largest transferring rate is $\Gamma_0/\hbar = 0.001$/fs for the definition of hybridization function, and $\lambda = 2$ Å. The electron affinity of the B atoms is 3.4011895 eV[59] (U_{atomic} in eq 1). Before activating any external electric field or electron transfer, our system is evolved (at 300 K) for 1 ns. We gather statistics from 100 trajectories of length 4 ns.

The electrochemical potential of the right electrode is fixed at −3.4000000 eV which is close to the electron affinity of the fluorine charge carriers (i.e., the B atoms); with this choice of electrochemical potential, there should be neither too many nor too few charged B^- atoms in the system. To simulate a change in voltage as applied to the system, we change only the electrochemical potential of the left electrode. We restrict ourselves to the nonresonant case that the electrochemical potential of the left electrode should be less than or equal to the electrochemical potential of the right electrode; thus, the electric field always points to the right (and electrons drift to the left). See the inset in Figure 3.[60]

4. RESULTS

We now analyze the model above exhaustively.

4.1. *I*–*V* Curve. In Figure 2 we plot the cumulative net electron transfer count as a function of time for 0.05 V. The blue and red curves are the cumulative count of net electron transfer into the left electrode and out of the right electrode, respectively. The steady-state current is the average slope of the curves at long time (i.e., after 1 ns). The difference between the two curves in Figure 2 is simply the average net charge of the system as a function of time. (Note that, at time 0, the system starts off charge neutral.)

The *I*–*V* data are shown in Figure 3. The solid curve with cross markers is data from our nonequilibrium simulation. While the overall curve is not linear, we do find a linear *I*–*V* relationship for small voltages. To better understand this linear regime, we compare our simulation data versus the linear

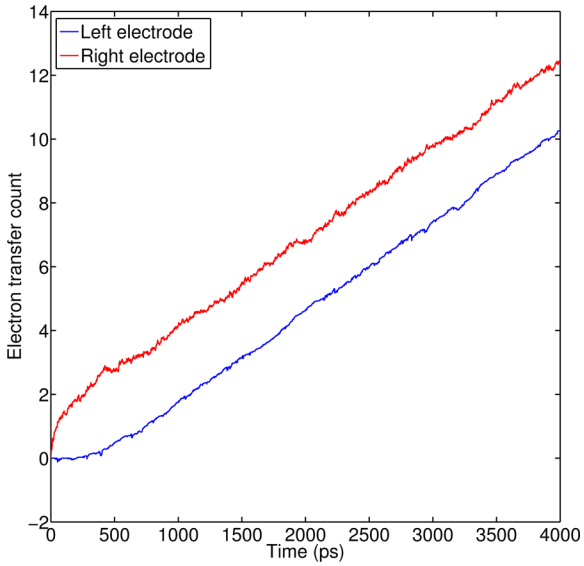

Figure 2. Cumulative net electron transfer count as a function of time at voltage 0.05 V. $\Gamma_0/\hbar = 0.001$/fs. For the left electrode (blue), the net electron count is the total number of electrons that have been *donated* by the solute up through time *t* minus the total number of electrons that have been *accepted* by the solute up through time *t*. For the right electrode (red), the net electron count is the total number of electrons that have been *accepted* by the solute up through time *t* minus the total number of electrons that have been *donated* by the solute up through time *t*. The difference between the red and blue curves is the net charge of the system. At early times, the net electron transfer count does not grow linearly, but after some transient time, a steady state is reached whereby the net electron transfer count grow linearly; the current can be calculated from the slope.

response prediction. To evaluate eq 23, we must first calculate N_q (the total number of charged solute atoms in the system) and $L_z^{(eff)}$ (the effective length of the box in the *z* direction).

- The average net charge of the system (N_q) can be calculated easily by measuring the difference between the two curves in Figure 2, assuming that the system starts off (at $t = 0$) with no charge.
- To estimate $L_z^{(eff)}$, we use the distance between the two major peaks in the position distribution for electron transfer, which is 53.2 Å. More details about these peaks in the electron transfer position distribution will be discussed in section 4.3.

In Figure 3, we plot two different versions of the linear response current eq 23. First, we plot the estimated current evaluated with the correct, steady-state nonequilibrium number of charged B^- atoms ($N_q(V)$) as in Figure 4; this plot recovers the basic plateauing of the I–V curve. Second, we plot the estimated current assuming the number of charged B^- atoms (N_q) is fixed and does not change with voltage (we choose the equilibrium ($V = 0$) density of B^- atoms in Figure 4); naturally, this plot gives a completely linear *I*–*V* relationship. All three curves agree at small voltage but both linear response curves consistently overestimate the current at large voltages.

There are two possible explanations for the overestimation by linear response. First, at large voltages, the charge carriers need not respond linearly to the voltage so the charge carriers might move slower than suggested by a linear response estimate.[61] Second, as the voltage increases, the time scale for charge carrier drift decreases. Eventually, if the box is small enough, this time scale will become comparable to the time

DOI: 10.1021/acs.jpcc.5b06655
J. Phys. Chem. C XXXX, XXX, XXX−XXX

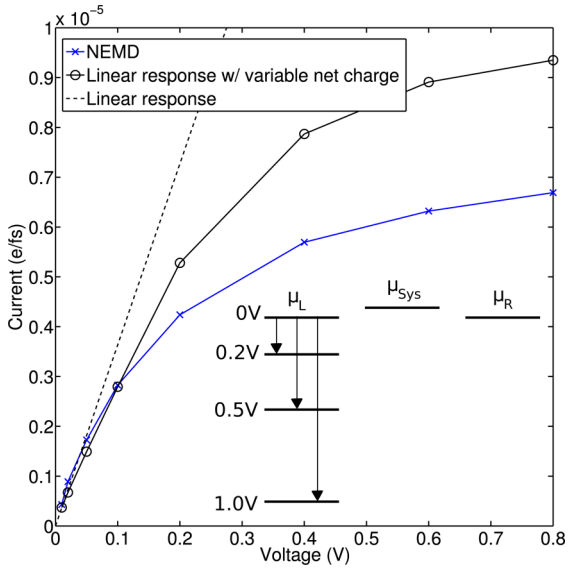

Figure 3. Current of the system as a function of the voltage applied. $\Gamma_0/\hbar$ = 0.001/*fs*. The blue curve marked by crosses is the result from our nonequilibrium simulation (NEMD = non-equilibrium molecular dynamics). The black curves are estimates from linear response theory (eq 23). The black curve with open circles calculates the current using a voltage-dependent number of B^- atoms (see Figure 4); the dashed black line assumes that the number of charged solute atoms is fixed (at zero voltage). At low voltages, linear response theory agrees with our nonequilibrium results quite well, but linear response overestimates the current in the case of high voltage. The inset is a schematic figure illustrating how a change in voltage is applied to the system: we keep a fixed electrochemical potential μ_R for the right electrode and we decrease the electrochemical potential of the left electrode μ_L: $\mu_L \leq \mu_R$, resonant transport is not considered. μ_{Sys} denotes the electrochemical potential of the system (which is close to the electron affinity of the B atoms).[60]

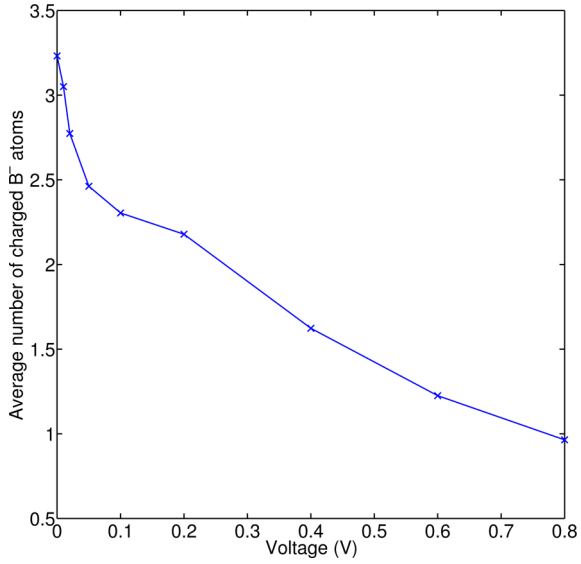

Figure 4. Average number of charged (B^-) atoms in the system as a function of voltage. $\Gamma_0/\hbar$ = 0.001/fs. This number decreases as the voltage increases because our voltage window is applied only to the left electrode (see the inset of Figure 3 for a schematic illustration).

scale of electron transfer at the leads. At the same time, however, eq 23 takes into account only the migration of charge carriers (i.e., mass transport) to calculate current. Thus, if the waiting time experienced by charge carriers (before an electron transfer event) is not small compared to the mass transport time, linear response theory will obviously overestimate the current.

These two explanations are not mutually exclusive; both could be present in our simulation box. In fact, in section 5.1, we will isolate how much each explanation contributes to the final current.[60]

4.2. Position of Charged Solute (B^-) Atoms. Electrochemistry is the study of chemical reactions at metal surfaces. Our ultimate interest in these simulations are the dynamics of charge injection to or from the metal surface, and how those charge injection dynamics are influenced by the local environment at the surface of the metal (including the ambient electric field). For example, there is currently a great deal of interest in studying the double layer of solvated ions near metallic surfaces.[62−68] To that end, a natural quantity for us to calculate is the distribution of charged ion position; this distribution is one measure of the solute's structure at the electrode interface and should be highly correlated with the dynamics of charge injection.

We have calculated this distribution in two different ways:

- We calculate a histogram while sampling ion positions from snapshots of nonequilibrium simulations.
- We fix a specific number of charged solute atoms for the system, and then construct a histogram while sampling ion positions from equilibrium simulations with a static electric field defined in eq 8.

These nonequilibrium and equilibrium distributions must be separately normalized for any comparison. *A priori*, we can expect two limiting cases. On the one hand, with weak enough coupling between the solution and the metal ($\Gamma_0 \to 0$), the equilibrium simulations must be equivalent to the nonequilibrium simulations if the charge is chosen correctly. On the other hand, if Γ_0 is large enough, we expect that ion density will be nearly uniform throughout the system, as current flows through the system.

Figure 5a shows the normalized distribution (of z coordinates) corresponding to negative ion position both for nonequilibrium and equilibrium simulation at a low voltage (0.02 V). For the equilibrium simulation, we inserted three B^- atoms into the simulation (which should be a good estimate; see section 4.1 and ref 69). From Figure 5a, we find that, even with small voltage, the equilibrium distribution is nearly the mirror opposite of the nonequilibrium distribution. Whereas the equilibrium distribution (with a small electric field pointing to the right) slightly favors negative ions sitting on the left, the nonequilibrium distribution slightly favors negative ions on the right. This discrepancy is easy to rationalize: for the nonequilibrium simulations alone, there is a small sink on the left which can accept electrons. (Note that the layer structure near both electrodes results simply from the Lennard-Jones interaction between the electrodes and the atoms; this layer structure is not terribly interesting.)

The differences between the equilibrium and nonequilibrium distributions in Figure 5a are amplified dramatically in the case of higher voltage. Figure 5b shows the normalized distributions at voltage 0.4 V. For the equilibrium simulations, we consider either one or two B^- atoms. In this figure, the electric field drives all of the charged B^- ions far to the left according to the equilibrium simulations; however, according to the nonequilibrium simulations, there is nearly a uniform density of

DOI: 10.1021/acs.jpcc.5b06655
J. Phys. Chem. C XXXX, XXX, XXX−XXX

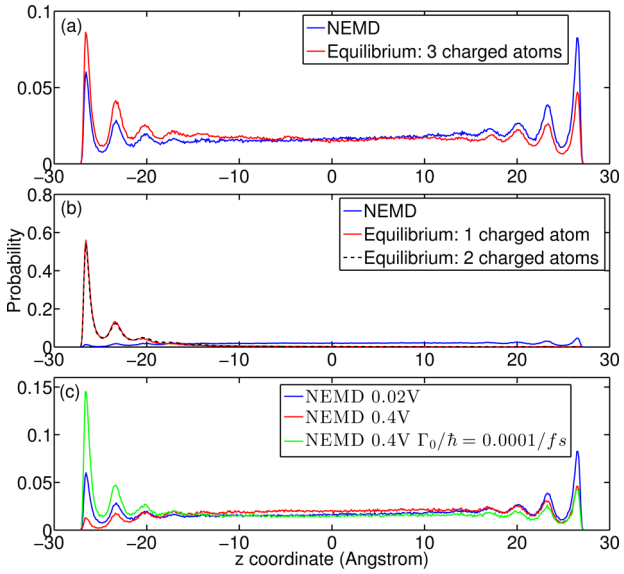

Figure 5. Normalized distribution of the z coordinates for the positions of the B^- ions using both nonequilibrium and equilibrium simulations. $\Gamma_0/\hbar$ = 0.001/*fs*. (a) Low voltage 0.02 V. (b) High voltage 0.4 V. (c) Comparison of low and high voltage. For the green curve, we reduce the hybridization Γ_0 by a factor of 10, $\Gamma_0/\hbar$ = 0.0001/fs. Equilibrium simulations with a number of B^- ions do not recover the nonequilibrium data at either low or high voltage, and the disagreement increases at higher voltage. Obviously, one cannot ignore the electron transfer rate at the electrodes for large enough Γ_0.

charged ions across the simulation box corresponding to a steady current through the liquid. Moreover, the density of anions decreases slowly as one approaches the sink on the left electrode. From this figure, one ascertains that there is far more screening of the external electric field in the equilibrium simulation as opposed to the nonequilibrium simulation. Whereas the B^- ions yield a strong electric field going from right to left in the equilibrium simulation (and against the external field), there is no such effect in the nonequilibrium simulations. In fact, in the nonequilibrium simulations, the B^- ions might even yield a small electric field going from left to right (in the same direction as the external field). In the future, it will be illuminating to insert bystander electrolytes into our simulation, as done by Voth et al. in ref 46, to model the screening effects of nonreactive ions.

In Figure 5c, we plot the nonequilibrium results from 0.02 and 0.4 V on the same y-scale. Here, we see the density of B^- ions near the left electrode is indeed far lower in the case of high voltage as compared to the case of low voltage. To understand the difference, note that there are two opposing effects here. On the one hand, with higher voltage, the B^- ions feel an external field pushing them to the left. On the other hand, however, with higher voltage, the electrons can also more easily escape into the left electrode once the B^- ion is close by. Apparently, in this regime, the second effect wins out. With a smaller Γ_0, however, the first effect does win out (as shown with the green cure in Figure 5c).The relative sizes of these two effects will be crucial for understanding solvent structure at the interfaces of polarizable and nonpolarizable electrodes.

4.3. Position of Electron Transfer. Lastly, we calculate the distribution of B or B^- ions at the time of electron transfer to help us to understand the $I-V$ curve atomistically. We will calculate this distribution in two different ways:

- For the nonequilibrium simulations, we simply make a histogram of all B or B^- positions at the time of electron transfer.
- For the equilibrium simulations, we calculate the equilibrium distribution of B or B^- positions (assuming there is no electron transfer, Γ_0 = 0), and we multiply that equilibrium distribution by the position dependent hybridization function defined in eq 11.

Figure 6 shows the normalized distribution of z coordinates for electron transfer events for both nonequilibrium and

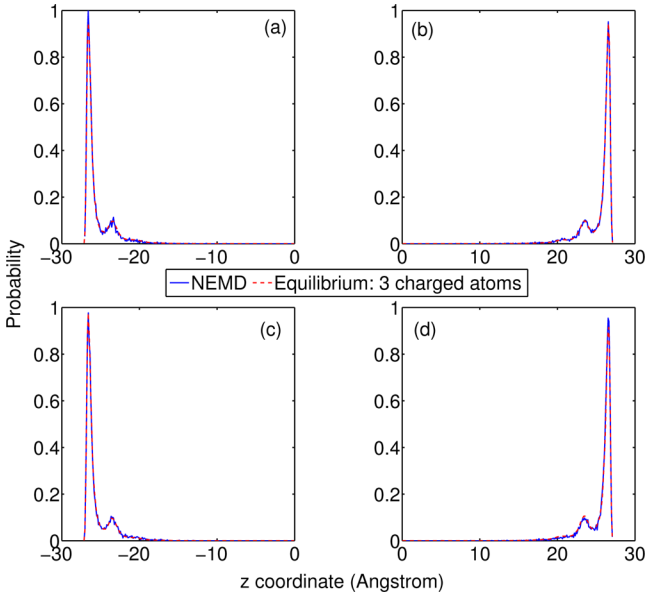

Figure 6. Normalized z-coordinate distribution of solute atoms during electron transfer events for both nonequilibrium and equilibrium simulations at voltage 0.02 V. $\Gamma_0/\hbar$ = 0.001/*fs*. Top: electron transfer from the electrodes to solute atoms. Bottom: electron transfer from solute atoms to the electrodes. Parts a and c are normalized on the left-hand side [-30, 0]; parts b and d are normalized on right-hand side [0, 30], The equilibrium simulation has three B^- atoms in the system. Clearly, an equilibrium simulation can recover the correct ratio of electron transfer events between different layers.

equilibrium simulations at low voltage (0.02 V). The equilibrium simulation contains three B^- atoms. Note here that, in each subplot, the distributions are normalized across either the left side of the box [-30, 0] or the right side of the box [0, 30] (rather than across the whole region [-30, 30] as in section 4.2). As can be seen from the figure, the equilibrium and nonequilibrium results agree nearly exactly. This agreement can be understood by investigating Figure 5a; even though the NEMD (blue) and equilibrium (red) curves are quantitatively different from each other, the two curves are very similar if renormalized on the left and right-hand sides, respectively. For both curves in Figure 5a, the innermost layer nearest the electrode has a larger magnitude than the second layer. Thus, at low voltage, an equilibrium approach can correctly recover some features of nonequilibrium electron transfer—even with relatively large Γ_0.

Whereas Figure 6 shows the equilibrium calculations can yield some useful information at low voltage, Figure 7[70] shows that at high voltage (0.4 V), the equilibrium simulations

DOI: 10.1021/acs.jpcc.5b06655
J. Phys. Chem. C XXXX, XXX, XXX−XXX

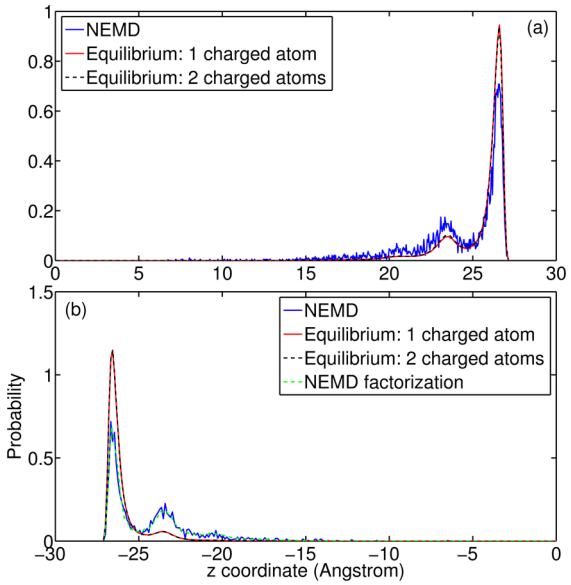

Figure 7. Voltage = 0.4V otherwise (a) Same as Figure 6b. (b) Same as Figure 6c. The equilibrium simulations have one and two B^- atoms in the system. Equilibrium simulations fail to recover the ratio of electron transfer events between different layers in such high voltage. However, as shown by the green dash curve labeled "NEMD factorization" in part b, the correct answer is recovered by multiplying the NEMD ion distribution in Figure 5b by $\Gamma(z)$ in eq 11.

do not recover even the relative ratio of electron transfer events occurring in the different layers of the solution. This mismatch is perhaps not surprising given the different ion densities in Figure 5b between the equilibrium and NEMD simulations. To confirm this interpretation, in Figure 7b, we plot a fourth curve, labeled "NEMD factorization" which is the NEMD ion distribution in Figure 5b multiplied by $\Gamma(z)$ in eq 11. The agreement between this fourth curve and the histogram of nonequilibrium electron transfer positions suggests that, at steady state, the dynamics of charge transfer into the electrode can sometimes be characterized completely by the simple steady-state distribution of negative ions—but calculating such a distribution does require performing nonequilibrium molecular dynamics.[71]

5. DISCUSSION

5.1. Nonlinearity and Electron Transfer. In section 4.1 (Figure 3), we found that linear response consistently overestimates the true NEMD current. Given that the current in an electrochemical cell is limited by two major processes, (*i*) mass transport of charge carriers and (*ii*) electron transfer at the electrode interface, one would like to isolate the contribution of each process to the total current.

To disentangle these effects, we now use a very simple model to calculate the current in our solution. We divide the set of all negatively charge B^- anions into those near the left electrode and those near the right electrode, and imagine the mechanism:

$$B_r^- \xrightarrow{k_f} B_l^- \xrightarrow{\Gamma_{ET}/\hbar} B_l \tag{24}$$

Here, $B_{l/r}^-$ denotes the number (density) of B^- atoms near the left and right electrodes, respectively, k_f represents the drift rate of B^- atoms from right to left as caused by the ambient electric field, and $\Gamma_{ET}/\hbar$ is the electron transfer rate as the B^- atoms inject an electron into the left electrode. The kinetic equations for this model are

$$\frac{dB_r^-}{dt} = -k_f B_r^- + S \tag{25a}$$

$$\frac{dB_l^-}{dt} = k_f B_r^- - \frac{\Gamma_{ET}}{\hbar} B_l^- \tag{25b}$$

$$\frac{dB_l}{dt} = \frac{\Gamma_{ET}}{\hbar} B_l^- \tag{25c}$$

where S represents a source current.

Now, the measurable current through the system is the electron transfer rate:

$$I = \frac{\Gamma_{ET}}{\hbar} B_l^- = \frac{\Gamma_{ET}}{\hbar} \frac{B_l^-}{B_r^- + B_l^-} (B_r^- + B_l^-) \tag{26}$$

At steady state (where $dB_l^-/dt = 0$ in eq 25b), we find $B_l^- = \hbar k_f B_r^-/\Gamma_{ET}$, so eq 26 becomes

$$I = \frac{\Gamma_{ET} k_f}{\Gamma_{ET} + \hbar k_f} (B_r^- + B_l^-) = \frac{\Gamma_{ET} k_f}{\Gamma_{ET} + \hbar k_f} N_q \tag{27}$$

Here N_q is the total number of B^- atoms in the system. Inverting eq 27, one finds a familiar equation:[72]

$$\frac{1}{I} = \frac{1}{k_f N_q} + \frac{\hbar}{\Gamma_{ET} N_q} = \frac{1}{I_{MT}} + \frac{\hbar}{\Gamma_{ET} N_q} \tag{28}$$

where I_{MT} is defined as the current of mass transport. Thus, within this model, we conclude that the total electron transfer time is the sum of the mass transport time plus the electron transfer time at the electrode. Note that eqs 25−28 neglect the backward electron transfer from the left electrode to neutral B atoms. This unidirectional flow of electrons should be valid only at large voltages according to eq 10; as such, we expect eq 28 may deviate from reality when the voltage is low.

eq 28 can be used to roughly disentangle the effects of a slow charge injection time versus the effect of a breakdown of linear response at high voltage. To make such an argument, we must specify N_q, Γ_{ET}, and I_{MT} in eq 28.

- First, for N_q, the number of B^- atoms is taken from Figure 4 (and the corresponding curve for smaller Γ_0).
- Second, for Γ_{ET}, one must use caution because the electron transfer rate in eq 11 is position dependent. Furthermore, from Figures 6 and 7, we know that electron transfer events occur over a range of atomic positions. For the sake of simplicity (and also for consistency with the definition of I_{MT}), we will estimate Γ_{ET} by (*i*) calculating the average position of electron transfer from the atoms to the left electrode $\langle z_{ET} \rangle$ and (*ii*) replacing $z = L_z/2 - |\langle z_{ET} \rangle|$ in eq 11 to calculate a single rate $\Gamma_{ET}/\hbar$ for a specific voltage.
- Third and finally, to demonstrate the limitations of linear response theory, we will calculate the mass transport current I_{MT} in two different ways:

1 We calculate the mass transport current according to linear response for ion flow, with eq 23.
2 We analyze the nonequilibrium (NEMD) velocity profile of the B^- atoms (i.e., velocity distribution in space)

DOI: 10.1021/acs.jpcc.5b06655
J. Phys. Chem. C XXXX, XXX, XXX−XXX

and calculate the average velocity in the z direction $\langle v_z \rangle$. We then calculate I_{MT} as

$$I_{MT} = \frac{N_q e \langle v_z \rangle}{L_z^{(eff)}} \tag{29}$$

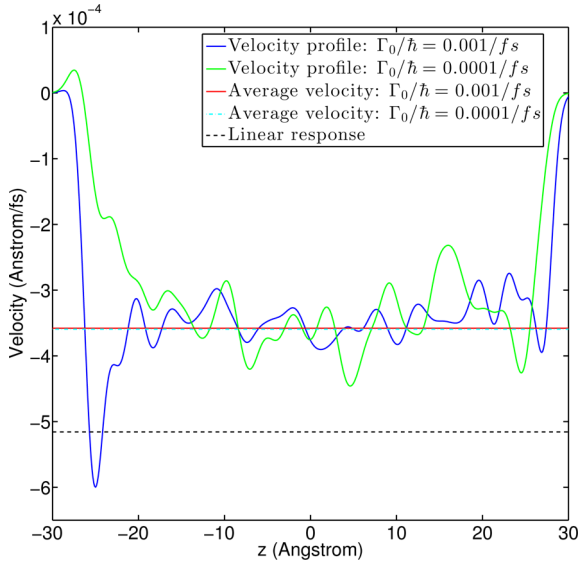

Figure 8. NEMD velocity profiles for a voltage of 0.8 V with $\Gamma_0/\hbar$ = 0.001 (blue curve) and $\Gamma_0/\hbar$ = 0.0001 (green curve). The velocity profiles have been smoothed by convolution with a Gaussian of width σ = 1 Å. At the edges of the box, near the electrodes, the ions have net velocity zero (as they must). The red solid line and the cyan dashed-dot line are the average velocities in the range [−10,10]Å for the two different Γ_0, respectively. Note that the average velocity in the middle of the system box is effectively independent of the value of Γ_0, and can be used to estimate the effective bulk drift velocity at high voltage. The black dashed line is the velocity calculated from linear response: $\langle v_z \rangle = u\mathcal{E}_z e$. The velocities are negative because the B^- atoms flow from right to left. The linear response result overestimates the velocity of the B^- atoms by approximately 31%.

A typical velocity profile is shown in Figure 8, where one can differentiate the nonequilibrium velocity from the linear response velocity. The average nonequilibrium velocity $\langle v_z \rangle$ in the middle region of the system is approximately 31% smaller than the linear response velocity.

For consistency with Γ_{ET}, in Figure 9 only, we redefine the effective length as $L_z^{(eff)} \equiv 2|\langle z_{ET} \rangle|$. Note that, with this definition, $L_z^{(eff)}$ will change a little bit depending on voltage.

In Figure 9, we plot the NEMD I−V curves corresponding to two different hybridization functions (on the left $\Gamma_0/\hbar$ = 0.001/fs, on the right $\Gamma_0/\hbar$ = 0.0001/fs). We also plot eq 28: for I_{MT} we use either eq 23 or the nonequilibrium velocity profile in Figure 8 with eq 29. For reference, we also include the raw linear response Green−Kubo estimates from Figure 3. At high voltage, Figure 9 isolates the corrections to the linear response current that arise from (*i*) calculating the velocity profile of a charge particle beyond linear response and (*ii*) including explicitly the waiting time for electron transfer.

This effectively completes our analysis of the *I*−*V* curves. The seasoned electrochemist might be surprised by the fact that, at high voltage, the current in our model is not limited by the diffusion of charge carriers as in a common electrochemical cell.[72] Instead, at large voltages, the current in Figure 9 is limited largely by charge injection. The explanation for this discrepancy is that our simulations above do not include supporting electrolyte. If there are no supporting electrolytes to form a double layer near the electrode and screen almost all of the electric field, charged ions move by drift (i.e., they are pushed by the electric field) instead of by diffusion. And, in such a case, mass transport is not limiting at high voltage and small length scales.

5.2. Interfacial Reaction. Before concluding, we now want to say a few words about chemical reactions at electrode interfaces. Clearly, such chemical reactions (that create and

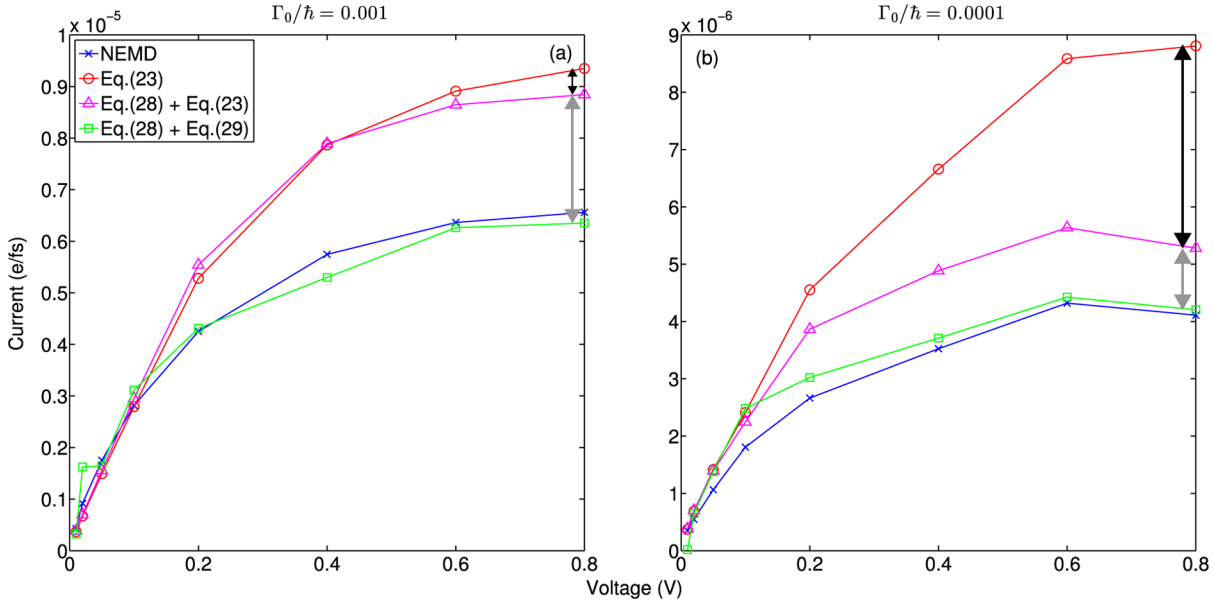

Figure 9. *I*−*V* curves calculated from NEMD simulations, linear response theory eq 23 (same as in Figure 3), and with a more sophisticated kinetic theory (eq 28). Two different $\Gamma_0/\hbar$ are used in the simulations, (a) 0.001/fs and (b) 0.0001/fs. In eq 28, I_{MT} is calculated in two different ways: either with eq 23 or with eq 29. The black arrows represent the errors in current that arise from ignoring the waiting time for electron transfer, and the gray arrows represent the errors in current that arise from assuming that ionic velocity follows linear response theory.

DOI: 10.1021/acs.jpcc.5b06655
J. Phys. Chem. C XXXX, XXX, XXX−XXX

break bonds) are missing in our treatment above. One simple means to incorporate such chemical reactions is to change the Lennard-Jones constants between charge carrying solute atoms and the electrodes, such that the charge carriers might be trapped on electrodes. The trapping of charge carriers at interfaces can be considered the simplest model of a chemical reaction whereby charge carriers become bonded to the electrode.

With this in mind, we have studied different Lennard-Jones potentials as obtained by changing the constant ε and thereby adjusting the depth of the potential well. The base (1×) ε is set as 0.2379 (as used above in section 3), and we consider Lennard-Jones constants ε of 2.379 (10×) and 11.895 (50×). In Figure 10,

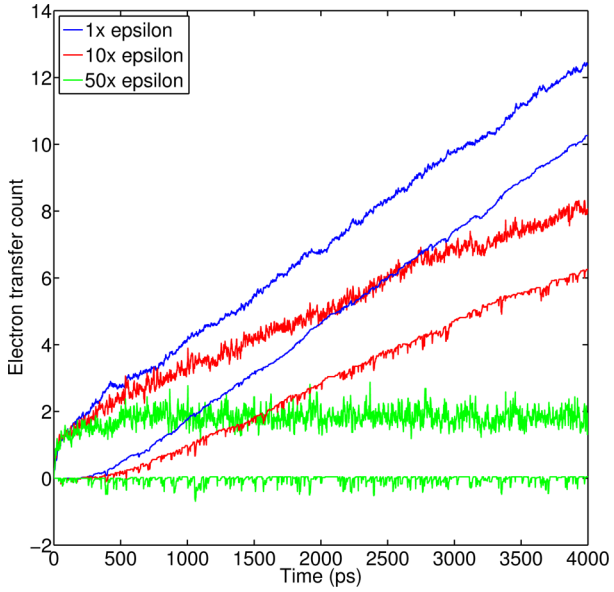

Figure 10. Cumulative net electron transfer count as a function of time at voltage 0.05 V. Curves with different colors correspond to different Lennard-Jones constants (ε) that measure the strength of the attraction between charge carriers and electrodes. ε is set as 0.2379, 2.379, and 11.895 for the blue, red and green curves, respectively. The upper blue curve corresponds to the net number of electron transfer events from the right electrode to the solute atoms and the lower blue curve corresponds to the net number of electron transfer events from the solute atoms to left electrode, etc. The slope of the curves is the current. As ε increases, charge carriers become trapped near the electrode and the current through the system decreases. When ε is large enough, the trapped charge carriers can no longer escape the potential well and the steady state current is effectively zero as indicated by the flat green curves.

we show the cumulative net electron transfer count as a function of time. We can see from the slope that, as ε increases, the current decreases. At 10×, we still measure a continuous current as the charge carriers are trapped only fleetingly; the B^- atoms manage to escape the attracted potential well of the electrode due to the collision with other atoms. However, when ε is very large (50× the base), the trapped charge carrier can no longer escape the trap of the electrode's potential and the electron transfer count becomes flat (i.e., there is no longer a current). One of the most exciting directions for future research will be modeling interfacial chemical reactions.

6. CONCLUSIONS AND FUTURE DIRECTIONS

In this paper, we have employed a nonequilibrium simulation to investigate the transport of electrons as mediated through an ionic solution. Figure 9 shows the key conclusions of this paper: in order to recover the results of a nonequilibrium simulation in the case of high applied voltage, we find it necessary to explicitly model both the nonequilibrium dynamics of the electron transfer processes and the nonlinear behavior of solute velocity.

Looking forward, we would next like to study larger simulations (e.g., those of Voth et al.[46,47]), including heterogeneous liquids made up of many polarizable solvent molecules and a host of electrolytes. While the model above was applied only for a collection of Lennard-Jones spheres, the approach should certainly be applicable to a variety of electrochemical systems, with arbitrarily complicated force fields. We would expect that, with polarizable waters as solvent, the electron-transfer dynamics will be sensitive to the time scale for water reorientation (∼1 ps) and that solvent structure and electrostatic shielding may greatly affect the probability for an electron hop. Furthermore, as is well-known, with electrolytes, a double layer will appear that will further shield the external electric field so that, even at reasonably high voltages, mass transfer is by diffusion rather than by drift. We are now beginning to run such calculations.

For very large systems, a direct study of charge transport may be difficult with the direct approach detailed in section 2. The reasons are 3-fold: First, because the electronic coupling is position dependent and the electron transfer event is probabilistic, our simulation time step (dt) is severely limited by the time scale for electron transfer and dt cannot be too large. Second, we waste a great deal of time calculating solvent reconfiguration and diffusion, especially since there are potentially more computationally efficient means to addresses such processes. If we want to handle large electrochemical cells, we expect methodological advances will be necessary to enhance the sampling of the electron transfer processes. Third and finally, one difficult question that will need to be addressed is how does the presence of polarizable solvent molecules affect the quantum mechanical lifetime (or broadening) of a charged ion (eq 11). This work is ongoing.

■ ASSOCIATED CONTENT

Supporting Information

The Supporting Information is available free of charge on the ACS Publications website at DOI: 10.1021/acs.jpcc.5b06655.

Histograms for the number of charged solute atoms in the system while in and out of equilibrium; schematic diagram of resonant charge transfer in ref 46(PDF)

■ AUTHOR INFORMATION

Corresponding Author

*(J.E.S.) E-mail: subotnik@sas.upenn.edu.

Notes

The authors declare no competing financial interest.

■ ACKNOWLEDGMENTS

This material is based upon work supported by the (U.S.) Air Force Office of Scientific Research (USAFOSR) PECASE award under AFOSR Grant No. FA9950-13-1-0157. J.E.S. acknowledges a Cottrell Research Scholar Fellowship and a David and Lucille Packard Fellowship. J.G.S. acknowledges support from NSF: MRSEC DMR-1120901 and CHE-1412496.

REFERENCES

(1) Bard, A. J. *Electrochemical Methods: Fundamentals and Applications*, 2nd ed.; Wiley: New York, 2001.

(2) Willard, A. P.; Reed, S. K.; Madden, P. A.; Chandler, D. Water at an Electrochemical Interfacea Simulation Study. *Faraday Discuss.* **2009**, *141*, 423−441.

(3) Nitzan, A. *Chemical Dynamics in Condensed Phases: Relaxation, Transfer and Reactions in Condensed Molecular Systems*, 1st ed.; University Press: New York, 2006; p 719.

(4) Dou, W.; Nitzan, A.; Subotnik, J. E. Surface Hopping with a Manifold of Electronic States. II. Application to the Many-Body Anderson-Holstein Model. *J. Chem. Phys.* **2015**, *142*, 084110.

(5) Tully, J. C. Molecular Dynamics with Electronic Transitions. *J. Chem. Phys.* **1990**, *93*, 1061−1071.

(6) Webster, F.; Rossky, P.; Friesner, R. Nonadiabatic Processes in Condensed Matter: Semi-Classical Theory and Implementation. *Comput. Phys. Commun.* **1991**, *63*, 494−522.

(7) Webster, F.; Wang, E. T.; Rossky, P. J.; Friesner, R. A. Stationary Phase Surface Hopping for Nonadiabatic Dynamics: Two-State Systems. *J. Chem. Phys.* **1994**, *100*, 4835−4847.

(8) Schwartz, B. J.; Bittner, E. R.; Prezhdo, O. V.; Rossky, P. J. Quantum Decoherence and the Isotope Effect in Condensed Phase Nonadiabatic Molecular Dynamics Simulations. *J. Chem. Phys.* **1996**, *104*, 5942−5955.

(9) Prezhdo, O. V.; Rossky, P. J. Mean-Field Molecular Dynamics with Surface Hopping. *J. Chem. Phys.* **1997**, *107*, 825−834.

(10) Fang, J.-Y.; Hammes-Schiffer, S. Improvement of the Internal Consistency in Trajectory Surface Hopping. *J. Phys. Chem. A* **1999**, *103*, 9399−9407.

(11) Fang, J.-Y.; Hammes-Schiffer, S. Comparison of Surface Hopping and Mean Field Approaches for Model Proton Transfer Reactions. *J. Chem. Phys.* **1999**, *110*, 11166−11175.

(12) Volobuev, Y. L.; Hack, M. D.; Topaler, M. S.; Truhlar, D. G. Continuous Surface Switching: An Improved Time-Dependent Self-Consistent-Field Method for Nonadiabatic Dynamics. *J. Chem. Phys.* **2000**, *112*, 9716−9726.

(13) Hack, M. D.; Truhlar, D. G. Electronically Nonadiabatic Trajectories: Continuous Surface Switching II. *J. Chem. Phys.* **2001**, *114*, 2894−2902.

(14) Jasper, A. W.; Hack, M. D.; Truhlar, D. G. The Treatment of Classically Forbidden Electronic Transitions in Semiclassical Trajectory Surface Hopping Calculations. *J. Chem. Phys.* **2001**, *115*, 1804−1816.

(15) Wong, K. F.; Rossky, P. J. Solvent-Induced Electronic Decoherence: Configuration Dependent Dissipative Evolution for Solvated Electron Systems. *J. Chem. Phys.* **2002**, *116*, 8429−8438.

(16) Wong, K. F.; Rossky, P. J. Dissipative Mixed Quantum-Classical Simulation of the Aqueous Solvated Electron System. *J. Chem. Phys.* **2002**, *116*, 8418−8428.

(17) Zhu, C.; Nangia, S.; Jasper, A. W.; Truhlar, D. G. Coherent Switching with Decay of Mixing: an Improved Treatment of Electronic Coherence for Non-Born-Oppenheimer Trajectories. *J. Chem. Phys.* **2004**, *121*, 7658−7670.

(18) Zhu, C.; Jasper, A. W.; Truhlar, D. G. Non-Born-Oppenheimer Trajectories with Self-Consistent Decay of Mixing. *J. Chem. Phys.* **2004**, *120*, 5543−5557.

(19) Jasper, A. W.; Truhlar, D. G. Electronic Decoherence Time for Non-Born-Oppenheimer Trajectories. *J. Chem. Phys.* **2005**, *123*, 064103.

(20) Subotnik, J. E.; Shenvi, N. A New Approach to Decoherence and Momentum Rescaling in the Surface Hopping Algorithm. *J. Chem. Phys.* **2011**, *134*, 024105.

(21) Shenvi, N.; Subotnik, J. E.; Yang, W. Simultaneous-Trajectory Surface Hopping: a Parameter-Free Algorithm for Implementing Decoherence in Nonadiabatic Dynamics. *J. Chem. Phys.* **2011**, *134*, 144102.

(22) Shenvi, N.; Subotnik, J. E.; Yang, W. Phase-Corrected Surface Hopping: Correcting the Phase Evolution of the Electronic Wavefunction. *J. Chem. Phys.* **2011**, *135*, 024101.

(23) Landry, B. R.; Subotnik, J. E. How to Recover Marcus Theory with Fewest Switches Surface Hopping: Add Just a Touch of Decoherence. *J. Chem. Phys.* **2012**, *137*, 22A513.

(24) Jaeger, H. M.; Fischer, S.; Prezhdo, O. V. Decoherence-Induced Surface Hopping. *J. Chem. Phys.* **2012**, *137*, 22A545.

(25) Subotnik, J. E.; Ouyang, W.; Landry, B. R. Can We Derive Tully's Surface-Hopping Algorithm from the Semiclassical Quantum Liouville Equation? Almost, but Only with Decoherence. *J. Chem. Phys.* **2013**, *139*, 214107.

(26) Parandekar, P. V.; Tully, J. C. Mixed Quantum-Classical Equilibrium. *J. Chem. Phys.* **2005**, *122*, 094102.

(27) Schmidt, J. R.; Parandekar, P. V.; Tully, J. C. Mixed Quantum-Classical Equilibrium: Surface Hopping. *J. Chem. Phys.* **2008**, *129*, 044104.

(28) Shenvi, N.; Schmidt, J.; Edwards, S.; Tully, J. Efficient Discretization of the Continuum Through Complex Contour Deformation. *Phys. Rev. A: At., Mol., Opt. Phys.* **2008**, *78*, 022502.

(29) Shenvi, N.; Roy, S.; Tully, J. C. Dynamical Steering and Electronic Excitation in NO Scattering from a Gold Surface. *Science* **2009**, *326*, 829−832.

(30) Shenvi, N.; Roy, S.; Tully, J. C. Nonadiabatic Dynamics at Metal Surfaces: Independent-Electron Surface Hopping. *J. Chem. Phys.* **2009**, *130*, 174107.

(31) Meyer, H.-D.; Miller, W. H. A Classical Analog for Electronic Degrees of Freedom in Nonadiabatic Collision Processes. *J. Chem. Phys.* **1979**, *70*, 3214−3223.

(32) Meyer, H.-D.; Miller, W. H. Analysis and Extension of Some Recently Proposed Classical Models for Electronic Degrees of Freedom. *J. Chem. Phys.* **1980**, *72*, 2272−2281.

(33) Stock, G.; Thoss, M. Semiclassical Description of Nonadiabatic Quantum Dynamics. *Phys. Rev. Lett.* **1997**, *78*, 578−581.

(34) Miller, W. H. Electronically Nonadiabatic Dynamics via Semiclassical Initial Value Methods. *J. Phys. Chem. A* **2009**, *113*, 1405−1415.

(35) Kim, H.; Nassimi, A.; Kapral, R. Quantum-Classical Liouville Dynamics in the Mapping Basis. *J. Chem. Phys.* **2008**, *129*, 084102.

(36) Nassimi, A.; Bonella, S.; Kapral, R. Analysis of the Quantum-Classical Liouville Equation in the Mapping Basis. *J. Chem. Phys.* **2010**, *133*, 134115.

(37) Kelly, A.; van Zon, R.; Schofield, J.; Kapral, R. Mapping Quantum-Classical Liouville Equation: Projectors and Trajectories. *J. Chem. Phys.* **2012**, *136*, 084101.

(38) Rekik, N.; Hsieh, C.-Y.; Freedman, H.; Hanna, G. A Mixed Quantum-Classical Liouville Study of the Population Dynamics in a Model Photo-Induced Condensed Phase Electron Transfer Reaction. *J. Chem. Phys.* **2013**, *138*, 144106.

(39) Kim, H. W.; Rhee, Y. M. Improving Long Time Behavior of Poisson Bracket Mapping Equation: a Non-Hamiltonian Approach. *J. Chem. Phys.* **2014**, *140*, 184106.

(40) Martínez, T. J.; Ben-Nun, M.; Levine, R. D. Multi-Electronic-State Molecular Dynamics: A Wave Function Approach with Applications. *J. Phys. Chem.* **1996**, *100*, 7884−7895.

(41) Ben-Nun, M.; Martínez, T. J. A Multiple Spawning Approach to Tunneling Dynamics. *J. Chem. Phys.* **2000**, *112*, 6113−6121.

(42) Yang, S.; Coe, J. D.; Kaduk, B.; Martínez, T. J. An "Optimal" Spawning Algorithm for Adaptive Basis Set Expansion in Nonadiabatic Dynamics. *J. Chem. Phys.* **2009**, *130*, 134113.

(43) Elste, F.; Weick, G.; Timm, C.; von Oppen, F. Current-Induced Conformational Switching in Single-Molecule Junctions. *Appl. Phys. A: Mater. Sci. Process.* **2008**, *93*, 345−354.

(44) Palla, P. L.; Pierleoni, C.; Ciccotti, G. Bulk Viscosity of the Lennard-Jones System at the Triple Point by Dynamical Non-equilibrium Molecular Dynamics. *Phys. Rev. E* **2008**, *78*, 021204.

(45) Mugnai, M. L.; Caprara, S.; Ciccotti, G.; Pierleoni, C.; Mareschal, M. Transient Hydrodynamical Behavior by Dynamical Nonequilibrium Molecular Dynamics: The Formation of Convective Cells. *J. Chem. Phys.* **2009**, *131*, 064106.

(46) Petersen, M. K.; Kumar, R.; White, H. S.; Voth, G. A. A Computationally Efficient Treatment of Polarizable Electrochemical

DOI: 10.1021/acs.jpcc.5b06655
J. Phys. Chem. C XXXX, XXX, XXX−XXX

Cells Held at a Constant Potential. *J. Phys. Chem. C* **2012**, *116*, 4903−4912.
(47) Cao, Z.; Peng, Y.; Voth, G. A. Ion Transport Through Ultrathin Electrolyte Under Applied Voltages. *J. Phys. Chem. B* **2015**, *119*, 7516−7521.
(48) Griffiths, D. J. *Introduction to Electrodynamics*, 2nd ed.; Prentice Hall: Englewood Cliffs, NJ, 1989; p 154.
(49) In practice, the reader will note that, if we do not include image charges, then eq 10 strikingly becomes independent of the electrochemical potentials, μ_L and μ_R, which is completely unphysical.
(50) Yeh, I.-C.; Berkowitz, M. L. Ewald Summation for Systems with Slab Geometry. *J. Chem. Phys.* **1999**, *111*, 3155−3162.
(51) Arnold, A.; De Joannis, J.; Holm, C. Electrostatics in Periodic Slab Geometries. I. *J. Chem. Phys.* **2002**, *117*, 2496−2502.
(52) de Joannis, J.; Arnold, A.; Holm, C. Electrostatics in Periodic Slab Geometries.II. *J. Chem. Phys.* **2002**, *117*, 2503−2512.
(53) Ballenegger, V.; Arnold, A.; Cerdà, J. J. Simulations of Non-Neutral Slab Systems with Long-Range Electrostatic Interactions in Two-Dimensional Periodic Boundary Conditions. *J. Chem. Phys.* **2009**, *131*, 094107.
(54) Allen, M., Tildesley, D. *Computer Simulation of Liquids*, 1st ed.; Oxford University Press: New York, 1987; p 385.
(55) Nosé, S. A Unified Formulation of the Constant Temperature Molecular Dynamics Methods. *J. Chem. Phys.* **1984**, *81*, 511−519.
(56) Swope, W. C.; Andersen, H. C.; Berens, P. H.; Wilson, K. R. A Computer Simulation Method for the Calculation of Equilibrium Constants for the Formation of Physical Clusters of Molecules: Application to Small Water Clusters. *J. Chem. Phys.* **1982**, *76*, 637−649.
(57) Frenkel, D., Smit, B. *Understanding Molecular Simulation: from Algorithms to Applications*, 2nd ed.; Academic Press: San Diego, CA, 2001; p 664.
(58) There are two subtleties that are worth comment. First, as is well-known, the velocity-velocity correlation function decays slowly (nonexponentially) and tails can be important.[73,74] In the context of our calculation—with a fixed box size in the z-direction—it is crucial to use the velocity-velocity correlation function in the unconstrained x, y directions for eq 16. Otherwise, anomalies will appear when the particles reach the box edge. Second, when evaluating the dynamics for the velocity-velocity correlation function, we will ignore Coulomb repulsion between charged B^- atoms. Our reasons are practical and 2-fold: (*a*) at any time, we never have more than 5 or 6 charged B^- atoms and usually fewer than 4;[69] (*b*) without periodic boundary conditions, as discussed above, the tails of the velocity-velocity correlation functions will be highly distorted in a confined box where, with Coulomb interactions, charged particles will inevitably repel one another at long times. By rerunning the entire simulation without any Coulombic repulsion at all, we have checked numerically that this neglect of Coulombic forces does not affect the conclusions of our paper regarding linear response.
(59) Blondel, C.; Delsart, C.; Goldfarb, F. Electron Spectrometry at the μeV Level and the Electron Affinities of Si and F. *J. Phys. B: At., Mol. Opt. Phys.* **2001**, *34*, L281−L288.
(60) Readers will notice that, while we observe plateauing in Figure 3, ref 46 by Voth et al. predicts that the linear relationship between current and applied voltage extends to quite a high voltage (without plateauing). These two findings are not contradictory. The subtlety here is the way in which one applies the external (i.e., source-drain) voltage across the electrochemical cell. In ref 46, the voltage is applied such that the left electrode has a potential of $+V/2$ and the right electrode has a potential of $-V/2$. In other words, as the source-drain voltage is increased, the potential of the left electrode is raised and the potential of the right electrode is decreased, so that for the large voltage, the current will proceed resonantly. In such a resonant regime, the average number of charged atoms should only increase with voltage. A picture of the relevant chemical potentials in ref 46 is shown in the Supporting Information. By contrast, as shown in the inset of Figure 3, we apply the external source-drain voltage differently (with one particular gate voltage). We simulate the external source-drain voltage by decreasing the electrochemical potential on only the left electrode. For our system (as indicated in Figure 4), the average number of charged atoms decreases when the voltage increases, which leads to plateauing in our I-V curves at high voltage in Figure 3, rather than a linearly increasing current (as found in ref 46). In a subsequent paper, we will consider the resonant case.
(61) After all, linear response theory works only when a perturbation is small compared to k_bT, which is approximately 0.026 eV when T = 300 K. Thus we can expect linear response theory to fail when the voltage is larger than 0.02 V.
(62) Cannes, C.; Cachet, H.; Debiemme-Chouvy, C.; Deslouis, C.; de Sanoit, J.; Le Naour, C.; Zinovyeva, V. a. Double Layer at [BuMeIm][Tf 2 N] Ionic Liquid-Pt or -C Material Interfaces. *J. Phys. Chem. C* **2013**, *117*, 22915−22925.
(63) Sha, M.; Dou, Q.; Luo, F.; Zhu, G.; Wu, G. Molecular Insights Into the Electric Double Layers of Ionic Liquids On Au(100) Electrodes. *ACS Appl. Mater. Interfaces* **2014**, *6*, 12556−12565.
(64) Cheng, J.; Sprik, M. The Electric Double Layer at a Rutile TiO2 Water Interface Modelled Using Density Functional Theory Based Molecular Dynamics Simulation. *J. Phys.: Condens. Matter* **2014**, *26*, 244108.
(65) Hughes, Z. E.; Walsh, T. R. Structure of the Electrical Double Layer at Aqueous Gold and Silver Interfaces for Saline Solutions. *J. Colloid Interface Sci.* **2014**, *436*, 99−110.
(66) Sugimoto, Y.; Kitazumi, Y.; Tsujimura, S.; Shirai, O.; Yamamoto, M.; Kano, K. Electrostatic Interaction Between an Enzyme and Electrodes in the Electric Double Layer Examined in a View of Direct Electron Transfer-Type Bioelectrocatalysis. *Biosens. Bioelectron.* **2015**, *63*, 138−144.
(67) Jänsch, T.; Wallauer, J.; Roling, B. Influence of Electrode Roughness on Double Layer Formation in Ionic Liquids. *J. Phys. Chem. C* **2015**, *119*, 4620−4626.
(68) Ma, K.; Forsman, J.; Woodward, C. E. Influence of Ion Pairing in Ionic Liquids On Electrical Double Layer Structures and Surface Force Using Classical Density Functional Approach. *J. Chem. Phys.* **2015**, *142*, 174704.
(69) This information can be found in the Supporting Information
(70) The keen observer will note that Figure 7 holds only two subplots, as opposed to the four subplots in Figure 6. This discrepancy exists because, in the case of high voltage, NEMD simulations do not allow for any electron transfer events from the left electrode to neutral solute atoms, while equilibrium simulation predict no B^- atom near the right electrode.
(71) And even then, this conclusion may not be general. Normally, one would at least need to consider the Fermi function in eq 10 and eq 14 in order for the green curve to match the blue curve in Figure 7b. In the present case, however, the voltage is large enough such that, once a B^- ion reaches the vicinity of the left electrode where $\Gamma(z)$ is non-negligible, one can safely ignore the Fermi function.
(72) Gileadi, E. *Physical Electrochemistry*, 1st ed.; Wiley-VCH: Weinheim, Germany, 2011.
(73) Alder, B. J.; Wainwright, T. E. Decay of the Velocity Autocorrelation Function. *Phys. Rev. A: At., Mol., Opt. Phys.* **1970**, *1*, 18−21.
(74) Levesque, D.; Ashurst, W. T. Long-Time Behavior of the Velocity Autocorrelation Function for a Fluid of Soft Repulsive Particles. *Phys. Rev. Lett.* **1974**, *33*, 277−280.

DOI: 10.1021/acs.jpcc.5b06655
J. Phys. Chem. C XXXX, XXX, XXX−XXX